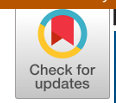

optica

Mid-infrared octave spanning supercontinuum generation to 8.5 μm in silicon-germanium waveguides

Milan Sinobad,[1,2,7] Christelle Monat,[1] Barry Luther-Davies,[3] Pan Ma,[3] Stephen Madden,[3] David J. Moss,[4] Arnan Mitchell,[2] David Allioux,[1] Regis Orobtchouk,[1] Salim Boutami,[5] Jean-Michel Hartmann,[5] Jean-Marc Fedeli,[5] and Christian Grillet[1,6]

[1]Université de Lyon, Institut des Nanotechnologies de Lyon (INL, UMR-CNRS 5270), Ecole Centrale de Lyon, 69130 Ecully, France
[2]CUDOS and School of Engineering, RMIT University, Melbourne, VIC 3001, Australia
[3]CUDOS, Laser Physics Centre, Australian National University, Canberra, ACT 0100, Australia
[4]Centre for Microphotonics, Swinburne University of Technology, Hawthorn, VIC 3122, Australia
[5]CEA-Leti, MINATEC Campus, 17 rue des Martyrs, 38054 Grenoble Cedex 9, France
[6]e-mail: christian.grillet@ec-lyon.fr
[7]e-mail: milan.sinobad@student.rmit.edu.au

Received 30 October 2017; revised 13 February 2018; accepted 14 February 2018 (Doc. ID 310213); published 27 March 2018

Efficient on-chip molecule and bio-agent detection can be achieved by accessing strong molecular absorption lines in the mid-infrared, but it requires high output power broadband mid-IR sources. Here, we report supercontinuum generation in an air-clad $Si_{0.6}Ge_{0.4}$/Si waveguide that emits a broad spectrum spanning from 3.0 μm to 8.5 μm. These waveguides have anomalous dispersion and low propagation loss (<0.4 dB/cm) in the mid-IR, which leads to a supercontinuum output with a high average power of more than 10 mW on-chip. The realization of broadband mid-IR sources with high spectral brightness makes the SiGe-on-Si platform promising for a wide range of applications.

OCIS codes: (320.6629) Supercontinuum generation; (190.4390) Nonlinear optics, integrated optics; (140.3070) Infrared and far-infrared lasers.

https://doi.org/10.1364/OPTICA.5.000360

1. INTRODUCTION

Molecule or bio-agent detection has a large number of applications in medicine, the food industry, environmental monitoring, and security [1,2]. If implemented in the form of low-cost, disposable on-chip sensors, it could lead to applications in early cancer diagnosis, real-time pollution detection, and food quality control [3]. To achieve high sensitivity, the molecules must be identified by measuring their fundamental rotational and vibration transitions that have strong characteristic "fingerprints" in the mid-infrared (mid-IR, between 3 μm and 20 μm) [4]. Mid-IR light sources with high spectral brightness are key enablers for such technologies. Various approaches have been used to achieve spectrally bright mid-IR sources, such as stand-alone quantum cascade lasers (QCLs) or tunable optical parametric amplifiers (OPAs) [5,6]. In this context, supercontinuum generation (SCG) operating via the nonlinear Kerr effect is particularly important. Indeed, this type of broad spectrum enables reliable molecule detection with high throughput by measuring, in parallel, the multiple and spectrally distinct absorption lines of a given molecule [7]. Demonstrations of such supercontinua with wide mid-IR bandwidth and high-power spectral density have already been reported in fibers [8–13] and recently in compact chalcogenide chip-based platforms [14]. The challenge is, however, to obtain an efficient and broadband mid-IR light source on a CMOS-compatible platform to leverage a mature and reliable fabrication technology and provide a path toward mass production.

High-performance linear and nonlinear photonic devices have been developed for telecom wavelengths, i.e., in the near-infrared, on the silicon-on-insulator (SOI) standard CMOS platform. A 350 nm spanning supercontinuum was achieved by pumping a low-loss SOI waveguide at 1.3 μm [15]. Despite the relatively large nonlinear gamma parameter (γ) in silicon at this wavelength, enabled by the combination of a large Kerr nonlinearity and small effective area, the nonlinear loss caused by two-photon absorption (TPA) significantly limited the bandwidth of the generated light [16]. By pumping at 2.1 μm, near the 2.2 μm TPA cutoff in silicon, a broader spectrum exceeding 990 nm in bandwidth could be generated [17], followed more recently by the demonstration of SCG up to 3.6 μm [18]. As an alternative to silicon, another group IV alloy, Si_xGe_{1-x}, which is also CMOS compatible, has proven to be an attractive nonlinear material for mid-IR applications [19–21]. The transparency window of SiGe expands more

deeply into the mid-IR (potentially up to 15 μm—well beyond the Si absorption limit—by employing Ge [22] or Ge-rich SiGe waveguides [23]), as compared to other CMOS-compatible platforms considered for operation in this wavelength region, such as silicon nitride [24] and Hydex [25,26]. In particular, a supercontinuum covering almost an octave (1.45–2.79 μm) in the shortwave infrared (SWIR) band was achieved in the SiGe-on-silica platform [27]. However, in addition to the nonlinear loss of the pump in the waveguide core, the silica cladding transparency eventually limits the SCG bandwidth up to 3.5 μm. Therefore, the SCG bandwidth generated on a SOI platform or its kin ($SiGe/SiO_2$) is bound at the short wavelength end by absorption and nonlinear loss in the core material and, at long wavelengths, by substrate absorption. Sophisticated SOI waveguide designs were proposed to overcome the latter limit [28]. By replacing silica with sapphire in the silicon-on-sapphire (SOS) platform, a supercontinuum covering more than an octave in the mid-infrared was demonstrated for the first time on any CMOS-compatible platform [29]. The spectrum was then limited to 6 μm by absorption in the sapphire substrate. This result represents the longest wavelength generated in a CMOS-compatible chip to date. Finally, the highest average power that has been generated via supercontinuum in the mid-IR to date is still less than 1 mW [29], largely because of linear and nonlinear losses in the waveguides.

Here, we demonstrate an octave-spanning, CMOS-compatible supercontinuum source in the mid-IR with high spectral brightness. We believe this is the first CMOS-compatible chip to exceed 6 μm, in fact reaching an unprecedented 8.5 μm. Our low-loss (<0.4 dB/cm) SiGe-on-Si waveguide platform enables high on-chip power of more than 10 mW—almost two orders of magnitude greater than previous demonstrations in SiGe [20]. By choosing a geometry for the SiGe waveguides patterned on a Si substrate with air as the upper cladding, we are able to appropriately engineer the waveguide dispersion while achieving a suitable trade-off between tight mode confinement and low effective area. The transparency of the silicon substrate from 1.1 to 8.5 μm [2,30] enables us to achieve a supercontinuum spectrum covering the entire 4 to 8 μm spectral band, where many atmospheric molecules have strong "fingerprints."

2. DEVICE DESIGN AND FABRICATION

Supercontinuum generated through soliton fission requires waveguides operating in a low and relatively flat anomalous dispersion regime [31,32]. Achieving low anomalous dispersion in waveguides with a low index contrast, such as those with a $Si_{0.6}Ge_{0.4}$ core and Si cladding (~0.16) [21], is challenging. Thus, we investigated SiGe/Si waveguides with a top air-cladding (see Fig. 1 inset). However, this vertically asymmetric waveguide geometry introduces additional constraints. First, it introduces a cutoff for the fundamental mode at long wavelengths. Second, the interaction between the evanescent field of the mode and the air cladding makes it more sensitive to the ambient environment and surface contamination, which might induce additional propagation losses. The main objectives of our design were to achieve low anomalous dispersion over a large bandwidth while strongly confining light in the waveguide core to minimize propagation losses. We also targeted a low effective area (A_{eff}) to achieve as high a nonlinear parameter ($\gamma = \omega_0 n_2 / c A_{\text{eff}}$) as possible. Our waveguides were designed to be pumped around 4 μm, which we previously identified as providing a good trade-off between high nonlinearity and low nonlinear losses (figure of merit—FOM) [21].

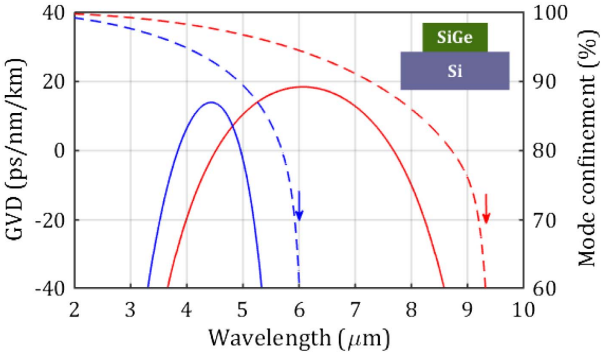

Fig. 1. Calculated group velocity dispersion (GVD) (solid lines) and mode confinement (dashed lines) of waveguide (1) in the TE mode (blue) and waveguide (2) in the TM mode (red). The arrows indicate the related cutoff wavelengths.

Here, we used air/SiGe/Si ridge waveguides with a slightly larger cross-sectional area than previously employed [21]. Because of the trade-off between effective area minimization (single-mode operation and maximized nonlinear parameter γ) and cutoff wavelength extension (low loss and strong mode confinement), we studied two designs: waveguide (1) with a 3.75 μm × 2.70 μm cross-section and waveguide (2) with a 6.0 μm × 4.2 μm cross-section. The key parameters of the two waveguides were calculated by a finite difference mode solver and are summarized in Table 1.

In essence, waveguide (1) yielded transverse-electric (TE) single-mode operation in the low anomalous dispersion regime, with a minimal effective area at 4 μm. Despite its relatively small effective area, we reached a mode confinement greater than 95% in the highly nonlinear SiGe core (Fig. 1). This, in turn, should improve the nonlinear parameter, and hence the conversion efficiency for SCG. The drawback of this design is the relatively short (~6 μm) cutoff wavelength for the fundamental TE waveguide mode that intrinsically limits the SC spectrum at long wavelengths. In contrast, waveguide (2) had a larger cross-sectional area and was designed to shift the cutoff wavelength of the fundamental transverse-magnetic (TM) mode beyond 8.5 μm (9.3 μm), enabling us to exploit, in principle, the full transparency window of the

Table 1. Summary of the Waveguide Parameters for the Two Designs[a]

Parameter	Waveguide (1) at 4 μm in TE	Waveguide (2) at 4.15 μm in TM
w (μm) × h (μm)	3.75 × 2.70	6.0 × 4.2
γ (W^{-1} m^{-1})	0.63	0.30
β_2 (ps/m^2)	-5.1×10^{-2}	1.1×10^{-1}
A_{eff} (μm^2)	6.25	14.0
Mode conf. (%)	95	98
1st ZDW (μm)	3.84	4.5
2nd ZDW (μm)	4.96	7.7
Cutoff λ (μm)	6.0	9.3

[a]From top to bottom: waveguide cross section, nonlinear parameter γ, second-order dispersion β_2, mode effective area A_{eff}, ratio of the mode energy in the waveguide core, 1st and 2nd zero dispersion wavelength (ZDW), and mode cutoff wavelength.

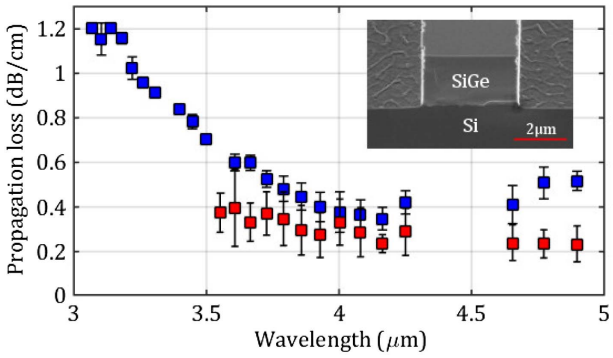

Fig. 2. Measured propagation loss for the TE mode of waveguide (1) (blue) and the TM mode of waveguide (2) (red). Inset: 3D scanning electron microscopy image of a cleaved SiGe 40%/Si waveguide.

SiGe/Si platform. However, we note that this larger waveguide is multimode at the pump wavelength (4.15 μm), and the effective area is double that of waveguide (1), which is expected to decrease the nonlinear conversion efficiency. The light confinement in the waveguide core was 98% and, most importantly, the dispersion of the TM fundamental mode was low and anomalous across a wider spectral range than for waveguide (1) (Fig. 1), which helped to maximize the bandwidth of the SC.

The two waveguides were fabricated on a 200 mm CMOS pilot line, using regular processes. First, 2.7 μm and 4.2 μm thick SiGe (40% Ge) layers were grown by epitaxy on top of Si substrates and encapsulated by 550 nm thick Si layers. Chemical-mechanical polishing was performed to remove the so-called surface cross-hatch, leaving a 50 nm thick Si layer. The waveguides were then patterned using deep ultraviolet photolithography followed by a deep reactive ion etching process (see Fig. 2 inset). More details about the fabrication procedure are included in Supplement 1.

3. EXPERIMENTAL RESULTS

We performed linear and nonlinear measurements on these two types of waveguides. By probing waveguides with three different lengths each (from 2 to 7 cm) under relatively low average powers (<1 mW), we measured the propagation losses using the cutback method. Measurements were performed using a tunable OPA delivering 7.5 ps long pulses at a 1.5 MHz repetition rate across a tunable wavelength range between approximately 3–5 μm. For waveguide (1), the propagation loss (Fig. 2) decreased from 1.2 to 0.5 dB/cm between 3 and 3.8 μm. We attribute the larger loss in the short wavelength range to absorption by the O–H bonds adsorbed on the waveguide surface and to the interaction of the higher-order modes with the waveguide sidewalls. Beyond 3.8 μm, where waveguide (1) was single mode, the measured propagation loss was relatively constant at 0.35–0.5 dB/cm. For waveguide (2), the measured propagation loss was equally flat versus wavelength (independent of the polarization, and not shown here), and reached a value as low as 0.23 dB/cm around 4.75 μm consistent with the larger cross-section area and tighter mode confinement (Fig. 2). To the best of our knowledge, this is the lowest propagation loss measured to date in any Si-based waveguides on a chip in the mid-IR. It is comparable to the recently inferred loss propagation in an Si microring [28].

Next, we probed the waveguides in the nonlinear regime by pumping them with sub-picosecond pulses using the experimental setup illustrated in Fig. 3. The 200 mW tunable OPA laser source (MIROPA-fs, Hotlight Systems) delivered ~200 fs pulses centered at either 4 μm [for waveguide (1)] or 4.15 μm [for waveguide (2)] at a 63 MHz repetition rate. We selected two different pump wavelengths to slightly adjust the pump to the two waveguide dispersions to operate as close as possible to the zero-dispersion wavelength (ZDW) for each waveguide, while avoiding the 4.15–4.30 μm CO_2 absorption wavelength band. Power and polarization-controlled optical pulses were coupled to the waveguide using a set of chalcogenide lenses. The generated SC spectrum was recorded using a liquid-nitrogen-cooled MCT (HgCdTe) photodetector positioned at the output of the spectrometer. In our setup, the impact of thermal noise was minimized using a lock-in detection technique. This setup was used in [14,20,21,29].

By pumping waveguide (1) with a 7 cm length at 4 μm in the anomalous dispersion regime close to the ZDW, more than an octave-spanning supercontinuum was achieved through the soliton fission process.

As illustrated in Fig. 4(a), which shows the different spectra measured for increasing coupled average power up to 16 mW, the SC extends between 2.63 and 6.18 μm, with a 3.55 μm bandwidth at −30 dB. The coupled power was estimated from the total chip transmission of −12.5 dB measured at low power, taking into account the chip propagation loss of −2.7 dB and assuming that the coupling loss was the same (−4.9 dB) at the input and output end facet of the waveguide.

Figure 5 shows the power contained in this broad supercontinuum (blue squares) at the end of our SiGe waveguides (which we refer to as "on-chip" SC power). It reached a value greater than 8 mW for 32 mW of coupled average power.

As can be seen in Fig. 4(a), the SC bandwidth achieved for waveguide (1) was limited by the fundamental mode cutoff at 6 μm. Next, we performed measurements on waveguide (2), which was designed to shift the cutoff wavelength up to 9.3 μm [i.e., beyond the silicon absorption limit at 8.5 μm (see Fig. 6—dashed red curve)]. Waveguide (2) was pumped at 4.15 μm, which is close to the first ZDW. We achieved a 1.4 octave-wide supercontinuum from 3 up to 8.3 μm (see Fig. 6), fully covering the 4–8 μm molecular fingerprint band. The generated spectrum was relatively flat across the whole wavelength range, as evidenced by the large −10 dB bandwidth of 4.9 μm (covering the 3.1–8 μm band), a value almost as wide

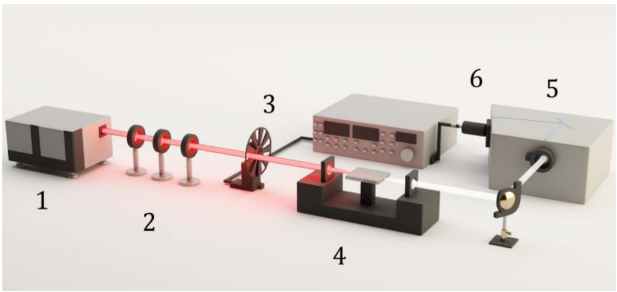

Fig. 3. Experimental setup used in SCG measurements. Elements are (1) tunable OPA, (2) optical waveplate and polarizers, (3) chopper connected to the lock-in amplifier, (4) sample and ChG lenses, (5) an optical spectrum analyzer (OSA), and (6) the MCT photodetector.

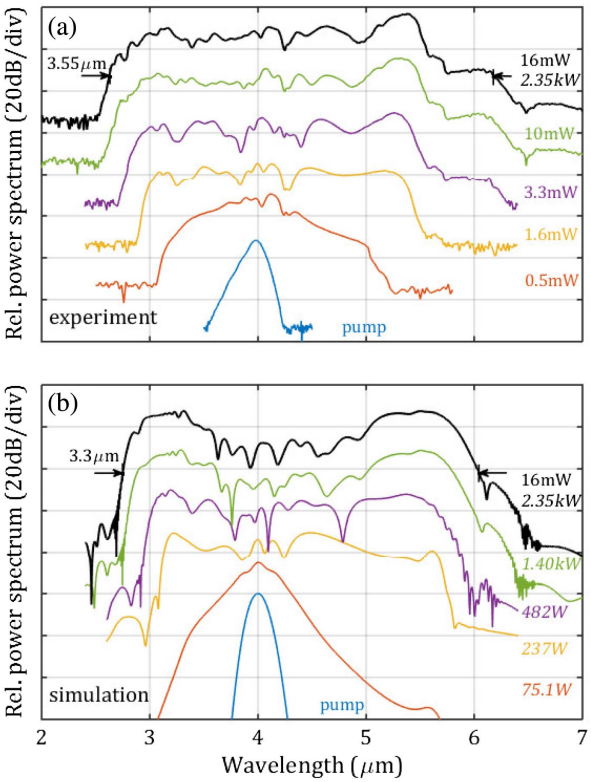

Fig. 4. (a) Spectra measured out of the 7 cm long waveguide (1) for increasing the coupled average power (quoted in regular font) and corresponding peak power (italic font). (b) Related spectra simulated by the split-step Fourier method for this waveguide geometry using the same peak power (italic font) as in (a). The arrows indicate the −30 dB bandwidth of the SC.

as the −30 dB bandwidth of 5.3 μm. The long wavelength boundary at −35 dB lies at 8.56 μm, limited by absorption in Si substrate, with an associated signal well above the noise level. The role of Si absorption is clearly seen with a drop of the generated SC spectrum intensity starting at ∼7 μm (see the green curve in Fig. 6).

As for waveguide (1), the SC signal is also spectrally bright, with a 3.85 mW power measured on the detector for 25 mW coupled average power, corresponding to 12.5 mW SC on-chip power (taking into account the ∼ − 5 dB coupling loss at the input/output facet).

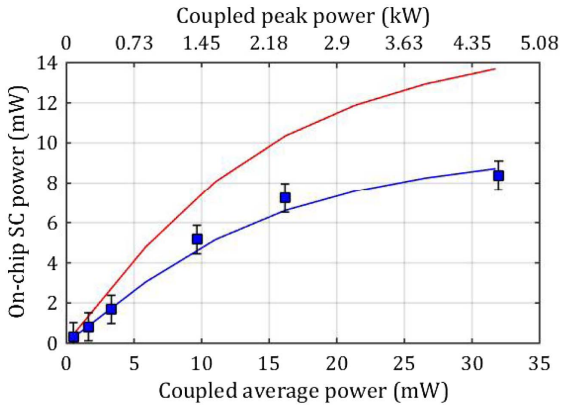

Fig. 5. On-chip SC power versus coupled average power measured for the 7 cm long waveguide (1) in TE at 4.0 μm (blue squares), simulated results for the 7 cm waveguide (blue line) and simulated results for a 2 cm long similar waveguide (red line).

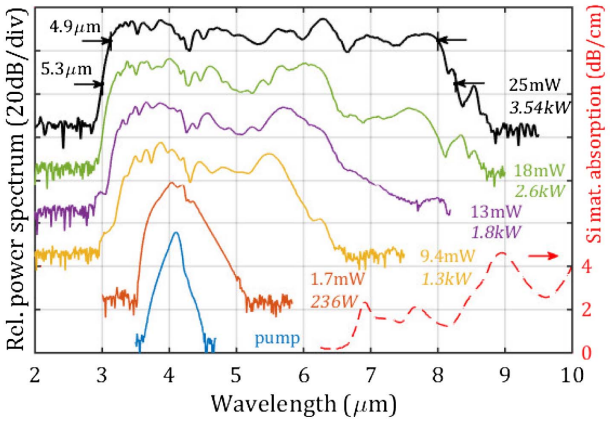

Fig. 6. Spectra measured out of the 7 cm long waveguide (2) pumped in TM at 4.15 μm for increasing coupled average power (indicated in regular font on the right side of each spectrum) and corresponding peak power (italic font). The dashed red curve highlights the absorption of crystalline silicon extracted from [30]. The two black arrows on the left highlight the −10 dB bandwidth and −30 dB bandwidth of 4.9 μm and 5.3 μm, respectively.

4. NUMERICAL MODELING AND DISCUSSION

To better understand our findings and clarify the enabling and limiting factors in these SCG results, we compared our experimental results to numerical modeling. Sub-picosecond pulse propagation in a SiGe waveguide can be described by the nonlinear Schrödinger equation (NLSE), which was solved numerically using the split-step Fourier method (SSFM). In our model, we included the linear loss, high- order dispersion (up to β_8), the nonlinear effect (Kerr and four-photon absorption), free-carrier absorption and dispersion, self-steepening, and Raman effects (see Supplement 1). Our model reproduced the experimental SC spectral signatures relatively well, as illustrated by the good agreement between the simulated [Fig. 4(b)] and measured [Fig. 4(a)] spectra of waveguide (1).

For waveguide (1), a 45% power conversion efficiency was achieved at 16 mW coupled average power. We similarly achieved reasonably good agreement between the simulated SC on-chip power generated at the end of the waveguide and the experimental data of Fig. 5. The best fit to the spectrum and SC on-chip power measurements of waveguide (1) were obtained for a γ of 0.63 $W^{-1}\,m^{-1}$ and a four-photon absorption coefficient α_{4PA} of 1.16×10^{-6} cm^5/GW^3. The inferred effective nonlinearity $n_2 = 2.5 \times 10^{-14}$ cm^2/W is in good agreement with the value reported earlier by our group [20]. Note that our estimate for the effective nonlinear absorption coefficient is more than an order of magnitude lower than that reported in c-Si [33]. This reemphasizes the potential of the SiGe platform for nonlinear optics in the mid-IR.

We simulated the propagation of 205 fs long, 2.35 kW coupled peak power (16 mW coupled average power) input pulses at a wavelength of 4 μm across the 7 cm long propagation distance (Fig. 7).

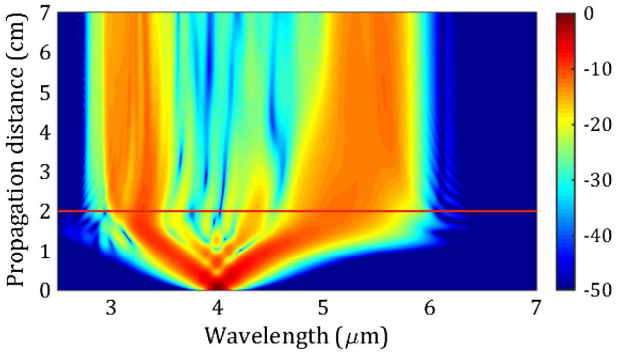

Fig. 7. Simulation of the pulse propagation along the 7 cm long waveguide (1) under 16 mW (2.35 kW) coupled (peak) average power at 4 μm.

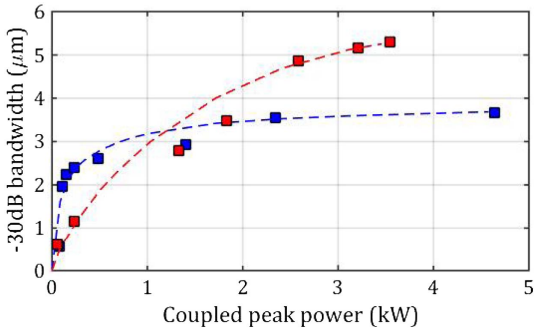

Fig. 8. Bandwidth at −30 dB versus coupled peak power experimentally measured for the waveguide (1) (blue) and waveguide (2) (red). The dashed curves are guides for the eye.

As described in [29], the spectral broadening shown in Fig. 7 is governed by higher-order soliton propagation in waveguide (1) pumped in the anomalous dispersion regime. This effect broadens the spectrum around the pump wavelength via the soliton fission process [31], while at the same time generating phase-matched dispersive waves in the normal dispersion region below 3.8 μm and beyond 5.0 μm. The calculated soliton number is 20 at a peak power of 2.35 kW giving a soliton fission length of 1.39 cm, which is in good agreement with Fig. 7. From these simulations, the spectrum appears completely broadened after a propagation distance of only 2 cm. The associated on-chip SC power calculated for a 2 cm long waveguide is plotted in Fig. 5, showing that we should be able to achieve an even higher 14 mW SC power (at 30 mW) with a high power conversion efficiency of 67% at 15 mW pump power in a shorter waveguide.

When comparing the results achieved in waveguides (1) and (2), we can see the impact of the γ parameter being twice as large in waveguide (1), as shown in Table 2. This effect is illustrated in Fig. 8, which shows the −30 dB bandwidth of the supercontinuum generated by the two waveguides versus coupled peak power. The SC bandwidth is higher for waveguide (1) at low pump power (<1 kW) while waveguide (2) performs better for higher pump powers, allowing us to achieve a much wider SC spectrum. This highlights the trade-offs of each design, depending on whether power consumption or bandwidth (particularly for applications requiring an octave span for self-referencing [34]) is most critical. We also found our design to be highly fabrication tolerant, with the dispersion remaining relatively constant when changing the waveguide width by 50 nm (see Supplement 1). This is well within the fabrication tolerance of the 200 mm pilot line and is significantly more robust than the previously reported silicon-on-sapphire approach [29].

When comparing with other Si based platforms used for the mid-IR (Table 2), the combination of dispersion engineering and low (linear and nonlinear) losses in our SiGe waveguides allowed us to achieve spectrally brighter SC signal.

The SC on-chip power of 12.5 mW at the end of our waveguide is indeed almost two orders of magnitude larger than that reported in previous work on SiGe waveguides [27] and an order of magnitude higher than for silicon-on-sapphire waveguides [29]. In particular, the low nonlinear loss allowed us to maintain high power conversion efficiency (the ratio of on-chip SC power P_{out} to coupled average power P_{in} was estimated at 0.5 compared to approximately 0.1 and 0.16 for silicon-on-sapphire and SiGe on silica, respectively [27,29]), even with high peak pump power, resulting in a spectrally bright SC signal.

Although we used slightly longer waveguides, our simulations pointed out that an even spectrally brighter (and similarly broad) SC on-chip signal could be achieved in a 2 cm long waveguide (i.e., a length comparable to previous work). We also achieved what we believe is the longest wavelength—8.56 μm—generated by any Si-based platform. Our results are competitive even with ChG waveguides, where spectrally bright (power conversion efficiency ∼0.6) and broad mid-IR SC were generated. However,

Table 2. Comparison of Current Results with Literature Data on Si-based Platforms Used for the Mid-IR and Results Achieved with the On-chip ChG Platform[a]

Platform	α (dB/cm)	l (cm)	γ $(Wm)^{-1}$	P_0/Pout	SCG Bandwidth
Our waveguides					
SiGe/Si (wg 1)	0.377 (4 μm)	7	0.63	2.35 kW/7.25 mW	2.6–6.2 μm
SiGe/Si (wg 2)	0.275 (4.15 μm)	7	0.30	3.5 kW/12.5 mW	3.0–8.3 μm
CMOS Compatible Platforms					
Si/Al_2O_3 [29]	1 ± 0.3 (3.7 μm)	1.6	8.2	1.82 kW/∼1 mW	1.9–5.5 μm
$SiGe/SiO_2$ [27]	2 (2.4 μm)	3	24.7	120 W/0.15 mW	1.4–2.8 μm
Si/SiO_2 [18]	N/A	2	∼50	15 W/–N/A	1.5–3.7 μm
Si/SiO_2 [17]	2.5 (2.12 μm)	2	150	12.7 W/–N/A	1.5–2.5 μm
On-Chip Chalcogenide Glass Platform					
GeAsSe/GeAsS [14]	0.6 (4.2 μm)	1.8	0.2	4.5 kW/20 mW	2.2–10.2 μm

[a]From left to right: propagation loss, waveguide length, extracted gamma parameter, coupled peak power (P_0)/on-chip SC power (P_{out}), and SC-generated −30 dB bandwidth. N/A stands for not available.

SiGe waveguides are fully CMOS compatible in terms of fabrication and yield a higher gamma parameter. Finally, in terms of power consumption, all of our results were achieved using a coupled peak power (P_0) comparable to that used to generate SC in the mid-IR (pumped around 4 μm) with SOS [29] and ChG [14], while being lower than in ChG fibers with similar cross sections [9,13].

5. CONCLUSION

We have demonstrated, in a CMOS-compatible waveguide platform, supercontinuum generation across a broad mid-IR wavelength range, spanning the entire 4–8 μm molecular fingerprint range. We used SiGe/Si dispersion engineered waveguides in the mid-IR to achieve a 1.4 octave wide spectrum, thanks to a careful design and tight mode confinement in the waveguide core, which yielded a propagation loss as low as 0.23 dB/cm. The low propagation loss combined with a low nonlinear loss allowed us to harness nonlinear effects in longer waveguides, resulting in a spectrally bright SC signal with more than 10 mW on-chip power corresponding to ∼50% power conversion efficiency. The broad anomalous dispersion profile of our waveguides yielded supercontinuum spectra extending to what we believe is the longest wavelength reported to date in any Si-based platform, reaching the c-Si absorption limit at 8.5 μm. Our results clearly establish silicon germanium-on-silicon as a promising platform for integrated nonlinear photonics in the mid-IR with the ability to operate at least up to 8.5 μm.

Funding. H2020 Marie Skłodowska-Curie Actions (MSCA) (631543); H2020 European Research Council (ERC) (GRAPHICS, 648546); Australian Research Council (ARC) (150104327, CE1101018); Agence Nationale de la Recherche (ANR) (MIRSICOMB, ANR-17-CE24-0028).

Acknowledgment. We acknowledge the support of the International Associated Laboratory in Photonics between France and Australia (LIA ALPhFA), and author Christelle Monat acknowledges the support of the Institut Universitaire de France.

See Supplement 1 for supporting content.

REFERENCES

1. R. Soref, "Mid-infrared photonics in silicon and germanium," Nat. Photonics **4**, 495–497 (2010).
2. L. Zhang, A. M. Agarwal, L. C. Kimerling, and J. Michel, "Nonlinear group IV photonics based on silicon and germanium: from near-infrared to mid-infrared," Nanophotonics **3**, 247–268 (2014).
3. B. Mizaikoff, "Waveguide-enhanced mid-infrared chem/bio sensors," Chem. Soc. Rev. **42**, 8683–8699 (2013).
4. Y.-C. Chang, "Design, fabrication and characterization of mid-infrared strip waveguide for laser spectroscopy in liquid environments" Ph.D. thesis (EPFL, 2012).
5. Y. Yao, A. J. Hoffman, and C. F. Gmachl, "Mid-infrared quantum cascade lasers," Nat. Photonics **6**, 432–439 (2012).
6. X. Liu, R. M. Osgood, Y. A. Vlasov, and W. M. J. Green, "Mid-infrared optical parametric amplifier using silicon nanophotonic waveguides," Nat. Photonics **4**, 557–560 (2010).
7. H. Pires, M. Baudisch, D. Sanchez, M. Hemmer, and J. Biegert, "Ultrashort pulse generation in the mid-IR," Prog. Quantum Electron. **43**, 1–30 (2015).
8. R. R. Gattass, L. B. Shaw, V. Q. Nguyen, P. C. Pureza, I. D. Aggarwal, and J. S. Sanghera, "All-fiber chalcogenide-based mid-infrared supercontinuum source," Opt. Fiber Technol. **18**, 345–348 (2012).
9. C. R. Petersen, U. Møller, I. Kubat, B. Zhou, S. Dupont, J. Ramsay, T. Benson, S. Sujecki, N. Abdel-Moneim, Z. Tang, D. Furniss, A. Seddon, and O. Bang, "Mid-infrared supercontinuum covering the 1.4–13.3 μm molecular fingerprint region using ultra-high NA chalcogenide step-index fibre," Nat. Photonics **8**, 830–834 (2014).
10. Y. Yu, B. Zhang, X. Gai, C. Zhai, S. Qi, W. Guo, Z. Yang, R. Wang, D.-Y. Choi, S. Madden, and B. Luther-Davies, "1.8–10 μm mid-infrared supercontinuum generated in a step-index chalcogenide fiber using low peak pump power," Opt. Lett. **40**, 1081–1084 (2015).
11. T. Cheng, K. Nagasaka, T. H. Tuan, X. Xue, M. Matsumoto, H. Tezuka, T. Suzuki, and Y. Ohishi, "Mid-infrared supercontinuum generation spanning 2.0 to 15.1 μm in a chalcogenide step-index fiber," Opt. Lett. **41**, 2117–2120 (2016).
12. C. R. Petersen, R. D. Engelsholm, C. Markos, L. Brilland, C. Caillaud, J. Trolès, and O. Bang, "Increased mid-infrared supercontinuum bandwidth and average power by tapering large-mode-area chalcogenide photonic crystal fibers," Opt. Express **25**, 15336–15348 (2017).
13. D. D. Hudson, S. Antipov, L. Li, I. Alamgir, T. Hu, M. El Amraoui, Y. Messaddeq, M. Rochette, S. D. Jackson, and A. Fuerbach, "Toward all-fiber supercontinuum spanning the mid-infrared," Optica **4**, 1163–1166 (2017).
14. Y. Yu, X. Gai, P. Ma, K. Vu, Z. Yang, R. Wang, D.-Y. Choi, S. Madden, and B. Luther-Davies, "Experimental demonstration of linearly polarized 2–10 μm supercontinuum generation in a chalcogenide rib waveguide," Opt. Lett. **41**, 958–961 (2016).
15. I.-W. Hsieh, X. Chen, X. Liu, J. I. Dadap, N. C. Panoiu, C.-Y. Chou, F. Xia, W. M. Green, Y. A. Vlasov, and R. M. Osgood, "Supercontinuum generation in silicon photonic wires," Opt. Express **15**, 15242–15249 (2007).
16. P. Koonath, D. R. Solli, and B. Jalali, "Limiting nature of continuum generation in silicon," Appl. Phys. Lett. **93**, 091114 (2008).
17. B. Kuyken, X. Liu, R. M. Osgood, R. Baets, G. Roelkens, and W. M. J. Green, "Mid-infrared to telecom-band supercontinuum generation in highly nonlinear silicon-on-insulator wire waveguides," Opt. Express **19**, 20172–20181 (2011).
18. R. K. W. Lau, M. R. E. Lamont, A. G. Griffith, Y. Okawachi, M. Lipson, and A. L. Gaeta, "Octave-spanning mid-infrared supercontinuum generation in silicon nanowaveguides," Opt. Lett. **39**, 4518–4521 (2014).
19. M. Brun, P. Labeye, G. Grand, J.-M. Hartmann, F. Boulila, M. Carras, and S. Nicoletti, "Low loss SiGe graded index waveguides for mid-IR applications," Opt. Express **22**, 508–518 (2014).
20. L. Carletti, P. Ma, Y. Yu, B. Luther-Davies, D. Hudson, C. Monat, R. Orobtchouk, S. Madden, D. J. Moss, M. Brun, S. Ortiz, P. Labeye, S. Nicoletti, and C. Grillet, "Nonlinear optical response of low loss silicon germanium waveguides in the mid-infrared," Opt. Express **23**, 8261–8271 (2015).
21. L. Carletti, M. Sinobad, P. Ma, Y. Yu, D. Allioux, R. Orobtchouk, M. Brun, S. Ortiz, P. Labeye, J. M. Hartmann, S. Nicoletti, S. Madden, B. Luther-Davies, D. J. Moss, C. Monat, and C. Grillet, "Mid-infrared nonlinear optical response of Si-Ge waveguides with ultra-short optical pulses," Opt. Express **23**, 32202–32214 (2015).
22. G. Z. Mashanovich, C. J. Mitchell, J. S. Penades, A. Z. Khokhar, C. G. Littlejohns, W. Cao, Z. Qu, S. Stanković, F. Y. Gardes, T. B. Masaud, H. M. H. Chong, V. Mittal, G. S. Murugan, J. S. Wilkinson, A. C. Peacock, and M. Nedeljkovic, "Germanium mid-infrared photonic devices," J. Lightwave Technol. **35**, 624–630 (2017).
23. J. M. Ramirez, V. Vakarin, C. Gilles, J. Frigerio, A. Ballabio, P. Chaisakul, X. Le Roux, C. Alonso-Ramos, G. Maisons, L. Vivien, M. Carras, G. Isella, and D. Marris-Morini, "Low-loss Ge-rich $Si_{0.2}Ge_{0.8}$ waveguides for mid-infrared photonics," Opt. Lett. **42**, 105–108 (2017).
24. R. Halir, Y. Okawachi, J. S. Levy, M. A. Foster, M. Lipson, and A. L. Gaeta, "Ultrabroadband supercontinuum generation in a CMOS-compatible platform," Opt. Lett. **37**, 1685–1687 (2012).
25. D. J. Moss, R. Morandotti, A. L. Gaeta, and M. Lipson, "New CMOS-compatible platforms based on silicon nitride and Hydex for nonlinear optics," Nat. Photonics **7**, 597–607 (2013).
26. D. Duchesne, M. Peccianti, M. R. E. Lamont, M. Ferrera, L. Razzari, F. Légaré, R. Morandotti, S. Chu, B. E. Little, and D. J. Moss, "Supercontinuum generation in a high index doped silica glass spiral waveguide," Opt. Express **18**, 923–930 (2010).

27. M. A. Ettabib, L. Xu, A. Bogris, A. Kapsalis, M. Belal, E. Lorent, P. Labeye, S. Nicoletti, K. Hammani, D. Syvridis, D. P. Shepherd, J. H. V. Price, D. J. Richardson, and P. Petropoulos, "Broadband telecom to mid-infrared supercontinuum generation in a dispersion-engineered silicon germanium waveguide," Opt. Lett. **40**, 4118–4121 (2015).
28. S. A. Miller, M. Yu, X. Ji, A. G. Griffith, J. Cardenas, A. L. Gaeta, and M. Lipson, "Low-loss silicon platform for broadband mid-infrared photonics," Optica **4**, 707–712 (2017).
29. N. Singh, D. D. Hudson, Y. Yu, C. Grillet, S. D. Jackson, A. Casas-Bedoya, A. Read, P. Atanackovic, S. G. Duvall, S. Palomba, B. Luther-Davies, S. Madden, D. J. Moss, and B. J. Eggleton, "Midinfrared supercontinuum generation from 2 to 6 μm in a silicon nanowire," Optica **2**, 797–802 (2015).
30. D. Chandler-Horowitz and P. M. Amirtharaj, "High-accuracy, midinfrared (450 $cm^{-1} \leq \omega \leq 4000\ cm^{-1}$) refractive index values of silicon," J. Appl. Phys. **97**, 123526 (2005).
31. J. M. Dudley, G. Genty, and S. Coen, "Supercontinuum generation in photonic crystal fiber," Rev. Mod. Phys. **78**, 1135–1184 (2006).
32. J. M. Dudley and J. R. Taylor, *Supercontinuum Generation in Optical Fibers*, 1st ed. (Cambridge University, 2010), p. 418.
33. X. Gai, Y. Yu, B. Kuyken, P. Ma, S. J. Madden, J. Van Campenhout, P. Verheyen, G. Roelkens, R. Baets, and B. Luther-Davies, "Nonlinear absorption and refraction in crystalline silicon in the mid-infrared," Laser Photon. Rev. **7**, 1054–1064 (2013).
34. S. A. Diddams, "The evolving optical frequency comb," J. Opt. Soc. Am. B **27**, B51–B62 (2010).